Talanta 188 (2018) 339–348

Contents lists available at ScienceDirect

Talanta

journal homepage: www.elsevier.com/locate/talanta

Sensitive nonenzymatic detection of hydrogen peroxide at nitrogen-doped graphene supported-CoFe nanoparticles

Mehboob Hassan, Yue Jiang, Xiangjie Bo*, Ming Zhou*

Key Laboratory of Nanobiosensing and Nanobioanalysis at Universities of Jilin Province, Key Laboratory of Polyoxometalate Science of Ministry of Education, National & Local United Engineering Laboratory for Power Batteries, Department of Chemistry, Northeast Normal University, Changchun, Jilin Province 130024, P.R. China

ARTICLE INFO

Keywords:
CoFe nanoparticles
Hydrogen peroxide
Nitrogen-doped graphene
Nonenzymatic sensor
Layered double hydroxides

ABSTRACT

In this work, a new enzymeless sensor for hydrogen peroxide (H_2O_2) was constructed by supporting CoFe nanoparticles on the nitrogen-doped graphene (CoFe/NGR). In this preparation, the graphene oxide (GO) is first used as substrate for the growth of CoFe layered double hydroxides (CoFe LDHs) through hydrothermal reaction. Then, the pyrolysis of CoFe LDHs/GO under NH_3 produces CoFe/NGR. By supporting CoFe nanoparticles on NGR support, the electrocatalytic performance of CoFe is dramatically improved because of high electric conductivity of NGR. Consequently, the combination of CoFe and NGR allows the nonenzymatic detection of H_2O_2. Compared with the unsupported CoFe nanoparticles, the CoFe/NGR displays high electrocatalytic activity towards H_2O_2, enabling a high sensitivity of 435.7 μA mM^{-1} cm^{-2} and low detection limit of 0.28 μM towards the reduction of H_2O_2. Especially, the attractive feature of low cost and outstanding analytical performance of CoFe/NGR suggest it great potential in electrochemical sensor and biosensor fabrication.

1. Introduction

Hydrogen peroxide (H_2O_2), described as the simplest peroxide, finds wide use in for pulp- and paper-bleaching, medical filed, waste-water treatment processes, and production of various organic peroxides [1]. In biological system, H_2O_2 is also a byproduct of large number of oxidase enzymes and is a ubiquitous oxidant present in all aerobic organisms. Accordingly, sensitive and accurate detection of H_2O_2 is important for biomedical and environmental monitoring. To achieve this goal, several analytical techniques, such as chemiluminescence [2,3] and fluorimetric method [4], have been used for H_2O_2 determination. In addition to these aforementioned ways, electrochemical sensors or biosensors are found to be capable for sensitive detection of H_2O_2 because of particular interest for their easy operation, portability, simplicity, and low-cost [1,5–12]. The enzyme-based H_2O_2 biosensors are one example for electrochemical sensors, which were constructed by immobilization of enzymes on the electrode surface [5,7]. As a result of specific enzyme activity, these enzyme-based H_2O_2 biosensors showed high performance, such as high sensitivity and excellent selectivity. Despite their high intrinsic activity, such H_2O_2 biosensors often suffer from poor stability due to the inherent instability and high cost of enzyme molecules. To address this problem, alternative H_2O_2 electrochemical sensors based on inorganic nanomaterials are reported to offer potential economic advantages and provide a desired way to overcome the high cost of enzymes and low stability. Recent rapid development in H_2O_2 electrochemical sensors has demonstrated the capability and stability of inorganic nanomaterials [1,2,13–22]. Among these alternative H_2O_2 sensors, transition metal nanomaterials are the very promising candidates for H_2O_2 electrochemical sensors because of their low cost, earth abundance and relatively easy preparation methods [8,13,14,17,21,23–33].

As mentioned above, transition metal nanomaterials have been widely used in H_2O_2 electrochemical sensors because of low cost and earth abundance. For example, CuO with dumbbell and grass-like morphologies were used as an electrode material for electrochemical sensing of H_2O_2 [34]. The result indicated that the nanostructuring method of CuO materials dramatically increased its performance by synergistically enhancing the effective electrode surface area and facilitating mass transport during electrochemical processes. In another work, Ni_7S_6 with flower-like morphology synthesized by a facile one-pot hydrothermal method were shown to be active for H_2O_2 sensing, exhibiting a wide linear range from 0.005 to 20.5 mM with a low detection limit of 0.15 μM and high sensitivity of 37.77 μA mM^{-1} cm^{-2} [30]. Other transition metal nanomaterials, including Fe_2O_3 [28,35], spinel [8,36,37], CuS [38], Cu oxides [32,39,40], perovskite [11,20], Mn oxides or hydroxides [16,25,29,41], CoP [42], NiO [17], Co_3N [43] and Cu_3N [44], also exhibited high activity toward the detection of H_2O_2. Although these transition metal nanomaterials show high

* Corresponding authors.
E-mail addresses: baoxj133@nenu.edu.cn (X. Bo), zhoum739@nenu.edu.cn (M. Zhou).

https://doi.org/10.1016/j.talanta.2018.06.003
Received 27 March 2018; Received in revised form 25 May 2018; Accepted 1 June 2018
Available online 04 June 2018

activity, their low electrical conductivity limits the charge transfer through the electrode surface and thereby restricts their analytical performance. Therefore, transition metal nanomaterial-based electrodes with higher electrical conductivity are preferred.

Noting the low electrical conductivity of transition metal nanomaterials, the electrical conductivity of transition metal nanomaterials can be improved by the synthesis of a composite containing a conductive additive, such as graphene (GR) [1,23–25] and carbon nanotubes [45]. The combination of the transition metal nanomaterials with a carbon support usually results in improvements in both stability and performance because directly anchoring the electrocatalyst to a conducting support allows a low-resistance electrical transport pathway. The electronic coupling between the conducting support and catalyst materials for synergistically improving the activity has been clearly demonstrated for MoS_2 nanoparticles synthesized directly on GR sheets [46], which exhibited enhanced performance and intrinsic electrocatalytic activity towards folic acid compared to unsupported MoS_2 particles. Similarly, the glucose oxidation and H_2O_2 reduction of Cu_2O/GR composites greatly exceeds that of Cu_2O nanocubes alone due to the superior electrical conductivity of GR support, resulting in linearity ranges of 0.3–3.3 mM and 0.3–7.8 mM for glucose and H_2O_2, respectively [40]. Building on the same principle, the activity of $NiCo_2O_4$ [47], FeN [48], ZrO_2 [49], Co_3O_4 nanoparticles [50], and CuO [24] is substantially enhanced when they are prepared as nanoparticles supported on carbon nanomaterials. The differences between transition metal nanomaterials and their composites in these recent studies highlight the electrochemical activities and stabilities of transition metal-based electrode materials can be improved by preparing on conductive support.

In addition to the enhancement of electric conductivity, alloying or mixing multiple transition metals is another attractive way to modify the electrochemical activity of transition metal-based electrode materials [51]. Generally, alloying or blending of transition metals has been demonstrated to tune the electronic states, interatomic spacing, and Fermi level energy, all of which could in turn affect the activity of the alloyed electrocatalyst toward the target analyte of interest [52,53]. This strategy has been experimentally exemplified in transition metal nanomaterials. For example, NiO/CuO/polyaniline exhibit significantly higher activity than NiO/polyaniline and CuO/polyaniline towards the oxidation of glucose, owing to favorable interactions between metal oxides and more active sites for electrocatalysis [54]. Similarly, CoCu alloyed nanoparticles grown on vertically aligned TiO_2 nanotube [55] and GR [56] possessed a high density of catalytic sites and benefitted from the excellent charge transport properties of alloyed nanoparticles, leading to high electrocatalytic activity towards glucose. Other transition metal alloys or mixed oxides, including CuCo alloyed dendrite [57], Cu_2O/NiO_x [58], Cu-Ag [59], NiO/CuO [60] also showed high analytical performance compared with their corresponding controls. As has been shown for the transition metal alloyed electrode materials, the incorporation of additional metal or metal oxide to a host compound is expected to alter the electrocatalytic performance due to alteration in its electronic properties, modifying their intrinsic activity.

In this work, a simple method is reported for preparation of CoFe nanoparticles/nitrogen-doped GR (CoFe/NGR) composites. First, the graphene oxide (GO) is used as substrate for the growth of CoFe layered double hydroxides (CoFe LDHs) through hydrothermal reaction. Under the NH_3 atmosphere, pyrolysis of CoFe LDHs/GO under NH_3 results in the formation of CoFe nanoparticles supported on NGR. Through the preparation of CoFe nanoparticles on NGR support, the electrocatalytic activity of CoFe is dramatically enhanced because of synergistic effects of Co and Fe elements and the high conductivity of NGR. The combination of CoFe and NGR ensures the nonenzymatic detection of H_2O_2 with high sensitivity, fast response, and low detection limit. Although GR or NGR have been reported as support for various nanoparticles, our methodology is special because: (1) alloying of the two transition metals modifies the electronic properties of CoFe nanoparticles, consequently leading to high intrinsic activity; (2) Additional attractive feature is the low cost and high earth-abundance of CoFe alloyed nanoparticles. Although the low cost and earth abundance of transition metal is not an important factor for use of small amount of nanomaterials, the cost the electrochemical sensor can be alleviated by using the less expensive transition metal-based nanomaterials compared with noble metal-based electrochemical sensors. The low cost, high earth-abundance and high activity endow CoFe/NGR as an electrochemical sensor for H_2O_2.

2. Experimental

2.1. Reagents and apparatus

$CoCl_2{\cdot}6H_2O$, $FeCl_3{\cdot}6H_2O$, Nafion and NaOH were purchased from Sigma-Aldrich. All other reagents (analytical grade) are used as received without further purification. The phosphate buffer saline (0.1 M, pH 7.4, PBS) was used as a supporting electrolyte. PBS was prepared with Na_2HPO_4, NaH_2PO_4 and 0.1 M KCl. The pH value of PBS solutions was adjusted by 0.1 M H_3PO_4 or 0.1 M NaOH. A stock solution of H_2O_2 (1.0 M) was prepared daily by diluting 30% (v/v) H_2O_2 into 10 mL with distilled water. The serum sample was obtained from the Hospital Attached to Northeast Normal University. The serum sample was diluted 2 and 10 times for electrochemical detection and titration method, respectively.

The X-ray diffraction (XRD) patterns were measured on the instrument of Rigaku X-ray D/max-2200vpc (Japan) operated at 20 mA and 40 kV using Cu Kα radiation (k = 0.15406 nm). The structure and morphology of samples are characterized by transmission electron microscopy (TEM, JEM-2100F TEM) and scanning electron microscope (SEM, Philips XL-30 ESEM) images. The Fe, Co, C, and N elements were tested by X-ray photoelectron spectroscopy (XPS, Thermo ESCA LAB spectrometer, USA). Electrochemical detection of H_2O_2 was performed on a CHI 660 C electrochemical workstation (CH Instruments, China) with a three-electrode configuration. The modified glassy carbon (GC, 3 mm diameter) electrode serves as a working electrode; Ag/AgCl in saturated KCl solutions works as reference electrode and a platinum wire is used as counter electrode. The electron transfer ability was characterized by electrochemical impedance spectroscopy (EIS) using a Par 2273 Potentiostats-Electrochemistry Workstation in 5 mM Fe $(CN)_6^{4-/3-}$ and 0.1 M KCl solutions from 0.1 Hz to 10.0 kHz at + 0.25 V. The calibration curve was constructed by plotting current versus concentration for standard solutions. The analytical results of CoFe/NGR-2 were validated by those determined by the classical potassium permanganate titration method. The sensor stability was evaluated by checking the current response or sensitivity before and after three weeks. The living cells were cultured according to our previous method [61].

2.2. Preparation of CoFe LDHs/GO and CoFe/NGR

GO was synthesized according to modified Hummers' method [62]. The preparation method of CoFe/NGR is illustrated in Scheme 1. The CoFe LDHs/GO was prepared were prepared by coprecipitation and aging method in the presence of GO. Then, the calcination of in CoFe LDHs/GO reducing atmosphere of ammonia gas leads to the decomposition of CoFe LDHs, nitrogen doping, and reduction of both CoFe LDHs and GO, yielding the product of CoFe/NGR. The $CoCl_2{\cdot}6H_2O$ and $FeCl_3{\cdot}6H_2O$ with different Co/Fe rations were added into 30 mL of GO solutions (1.6 mg L^{-1}). The total amount of 10 mM for $CoCl_2{\cdot}6H_2O$ and $FeCl_3{\cdot}6H_2O$ is kept same. After ultrasonication for 2 h, the pH value of above mixture was adjusted to 10.00 with 0.1 M NaOH. Then, the solution was transferred into autoclave with capacity of 60 mL and the autoclave was maintained at 100 ℃ for 6 h. The product was collected by configuration and frozen drying. Finally, the product was calcined in NH_3 flow at 800 ℃ for 3 h. The NGR was prepared with same procedure

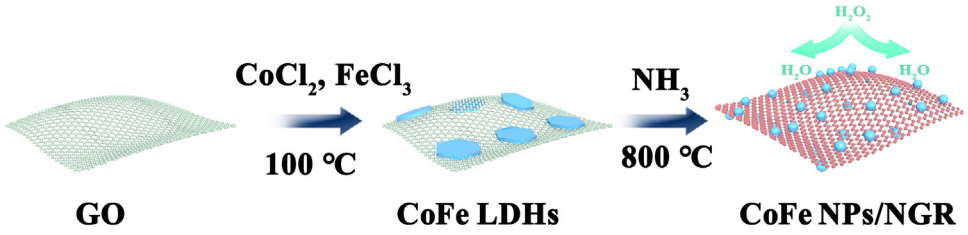

Scheme 1. Preparation pathway for CoFe/NGR-2.

except without the LDHs. $Co(OH)_2$/GO and $Fe(OH)_3$/GO were synthesized using the same method. In this work, the Co:Fe ratio of 2:1, 1:1, and 1:2 are defined as CoFe/NGR-1 (CoFe LDHs/GO-1), CoFe/NGR-2 (CoFe LDHs-2, CoFe-2 and CoFe LDHs/GO-2), and CoFe/NGR-3 (CoFe LDHs/GO-3), respectively.

2.3. Electrode fabrication

Different samples (3 mg) were dispersed into Nafion solution (0.5 wt %, 1 mL). After ultrasonication for 30 min, a well-dispersed solution was obtained. After carefully polishing the GC electrode with Al_2O_3 powder, the sample was dropped onto the electrode surface and then the electrode was dried in the air. To remove the interference from oxygen, the PBS solution was bubbled with highly pure nitrogen gas for 10 min.

3. Results and discussion

3.1. Characterization of CoFe/NGR

First, the composition of different product was examined by XRD method. As shown in Fig. 1. The CoFe LDHs-2 show characteristic diffraction peaks at 11.26°, 22.73°, and 35.60°, corresponding to the (003), (006), and (009) planes of CoFe LDHs [63]. After supporting the CoFe LDHs-2 on GO, CoFe LDHs/GO-2 exhibits the similar XRD patterns as the CoFe LDHs-2. However, it should be noted that the typical XRD peak at around 10° disappears because the regular layered structure of GO has been destroyed by CoFe LDHs-2. Upon thermal pyrolysis in NH_3 flow, the $Co(OH)_2$ is converted to Co NPs/NGR as evidenced by three typical XRD peaks for metallic Co. In contrast, the $Fe(OH)_3$/GO is changed to Fe_2N/GR composites. As for the CoFe/NGR-2, the XRD pattern shows three peaks at 44.85°, 65.45°, and 83.01° which are respectively assigned to (110), (200), and (211) of CoFe. The CoFe-2 without the GO also exhibits the same composition of CoFe after thermal pyrolysis.

In Fig. 2, the morphology of CoFe/NGR-2 was further studied by

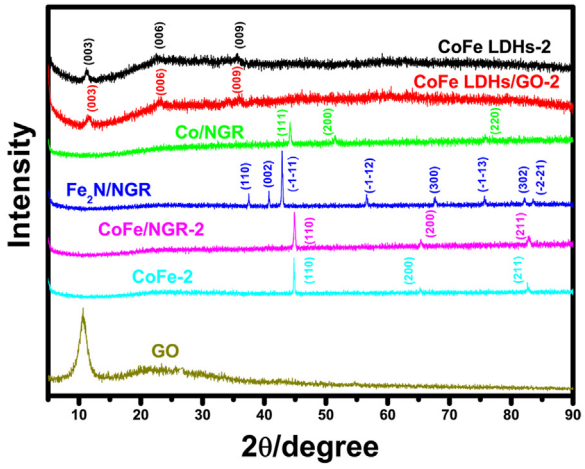

Fig. 1. XRD patterns of GO, CoFe LDHs-2, CoFe LDHs/GO-2, Co/NGR, Fe_2N/NGR, CoFe/NGR-2, and CoFe-2.

SEM method. The GO exhibits the layered structure in Fig. 2A. In Fig. 2B, CoFe-2 with the thickness of around 24.1 nm are synthesized. In the presence of GO (Fig. 2C), CoFe LDHs-2 are supported on the surface of GO, as marked in Fig. 2D. Similarly, CoFe LDHs-1 (Fig. S1B) and CoFe LDHs-3 (Fig. S1C) are also well supported on GO. As shown in the Fig. S1A and 1D, $Co(OH)_2$ and $Fe(OH)_3$ are supported on GO. After thermal reduction, the NGR shows a thin layered structure (Fig. 2E). After pyrolysis, aggregation of CoFe nanoparticles is found in CoFe-2 (Fig. 2F). In contrast, many CoFe-2 nanoparticles are facilely deposited on the NGR (CoFe/NGR-2), reflecting the vital role of NGR in improving the dispersion of CoFe-2 nanoparticles (Fig. 2G-H). The NGR also improves the dispersion of nanoparticles in CoFe/NGR-1 (Fig. S1F) and CoFe LDHs-3 (Fig. S1G). As shown in Fig. S1E and S1H, the Co and Fe_2N are also uniformly deposited in NGR, respectively. Additionally, the C, N, Fe, and Co elemental mappings of CoFe/NGR-2 also validate the doping of N and the supporting CoFe-2 nanoparticles. The well dispersion of Fe, Co, and N elements in CoFe/NGR-2 suggest the doping of N elements and uniformly distribution of CoFe-2 nanoparticles (Fig. 3). From the EDS result in Fig. 3F, the presence of Fe, Co and N also supports the conclusion of elemental mappings. The Co and Fe contents are found to be 16.93 at% and 17.97 at%, respectively, close to the initial ratio of 1:1. The N content is estimated to be 1.53 at%. The structure of CoFe-2 nanoparticles in CoFe/NGR-2 was further confirmed by TEM image. The NGR exhibits chiffon-like transparent film (Fig. 4A). In Fig. 4B-C, CoFe-2 nanoparticles with average size of 15 nm are facilely supported on GR. From the HRTEM image in Fig. 4D, the lattice of 0.20 nm corresponds to the (110) plane of CoFe, which is well accordance with XRD result.

The composition of Co/NGR, CoFe/NGR-2, and Fe_2N/NGR was studied by XPS method. First, the evolution of C 1 s spectra (Fig. S2) reflects the efficient removal of oxygen-related functional groups and thermal reduction of GO in NH_3 flow. Compared with Co/NGR (Fig. 5A-C) and Fe_2N/NGR (Fig. 5D-F), the presence of Co 2p (Fig. 5G) and Fe 2p (Fig. 5H) signals of CoFe/NGR-2 suggest the deposition of CoFe-2 nanoparticles. The fitted peaks of Co 2p spectrum at around 778.5, 780.6, 782.2 and 785.2 eV are assigned to the metallic Co, Co^{3+}, Co^{2+}, and satellite peak, respectively. Generally, the Co-based materials are vulnerable to surface oxidation when the Co-based materials are exposed in the air. Additionally, the XPS is surface characterization method, thus leading to the enrichment of Co oxide on the surface composition. The Fe 2p spectrum shows two peaks at 712.0 and 724.3 eV, corresponding to the Fe 2p3/2 and Fe 2p1/2, respectively. The N 1 s in Fig. 5C and I can be deconvoluted into four components at 397.8, 399.8, 401.2, and 402.5, which correspond to pyridinic N, pyrrollic N, graphitic N, and oxidized nitrogen compounds, respectively. In addition to the four configurations, the presence of N-Fe compounds for Fe_2N/NGR (Fig. 5F) at 398.8 eV suggests the formation of Fe_2N on NGR. The N content for Co/NGR, CoFe/NGR-2, and Fe_2N/NGR are calculated to be 1.79, 1.62, and 1.67 at%.

3.2. Electrochemical catalysis of H_2O_2 at CoFe/NGR-2

As noted above, the CoFe-2 nanoparticles are supported on NGR. Because of the high conductivity of NGR and the alloying of CoFe-2 nanoparticles, the CoFe/NGR-2 may integrate the catalytic properties from both composites. In this work, the electrocatalytic activity of

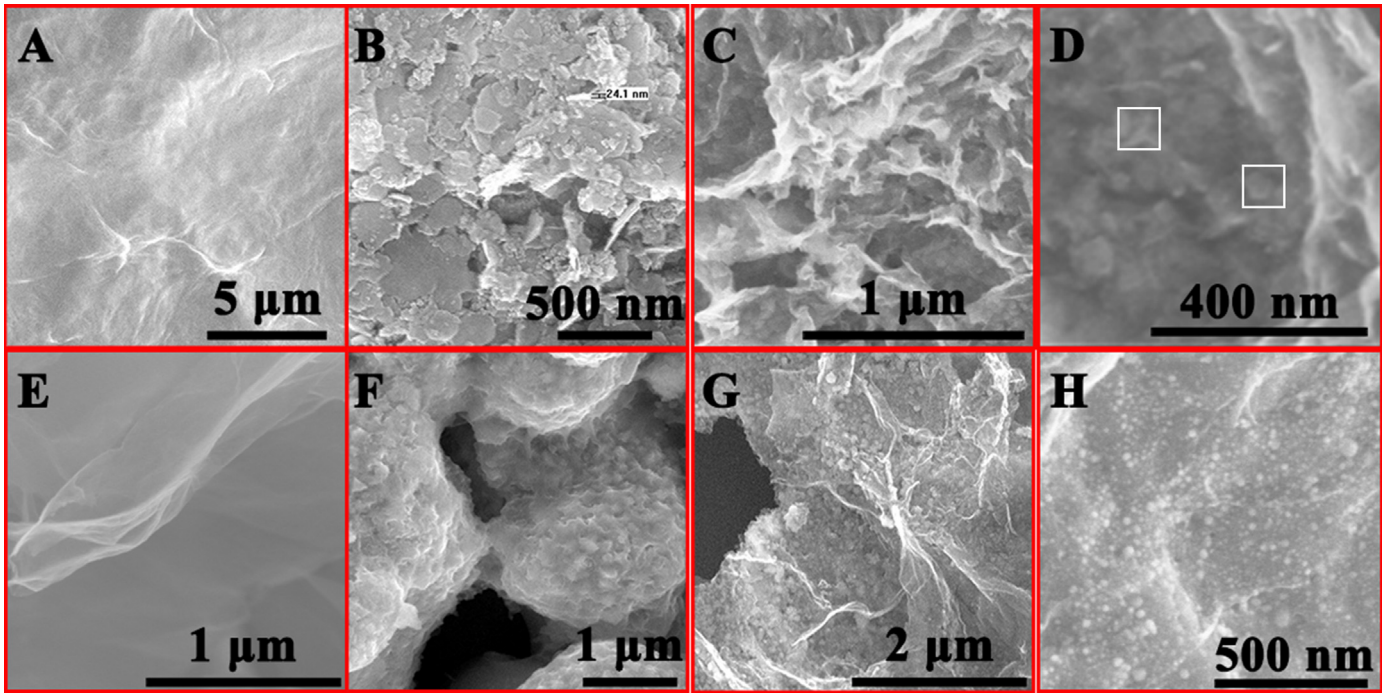

Fig. 2. SEM images of (A) GO, (B) CoFe LDHs-2, (C and D) CoFe LDHs/GO-2, (E) NGR, (F) CoFe-2, and (G and H) CoFe/NGR-2.

CoFe/NGR-2 towards the H_2O_2 reduction was compared with CoFe-2 nanoparticles, NGR, Co/NGR, Fe_2N/NGR, and CoFe LDHs/GO-2 in Fig. 6. The CoFe-2, CoFe LDHs/GO-2, and NGR present relatively low activity towards the reduction of H_2O_2. As can be seen from Fig. 6, a lowering of overvoltage and signal amplification is observed at the CoFe/NGR-2 electrode compared to those of Co/NGR and Fe2N/NGR. The cathodic peak potential for H_2O_2 is around − 0.26 V and the reduction current is about − 137.3 µA at the CoFe/NGR-2, compared to − 0.30 V and − 86.3 µA at Co/NGR electrode and − 0.38 V and − 33.9 µA at Fe_2N/NGR. This observation reflects the superior performance of CoFe/NGR-2 over Co/NGR and Fe_2N/NGR as electrode material. In comparison with CoFe-2, CoFe LDHs/GO-2 and NGR, three CoFe/NGR electrodes show higher activities for the reduction of H_2O_2 with CoFe/NGR-1, CoFe/NGR-2, and CoFe/NGR-3 exhibiting current

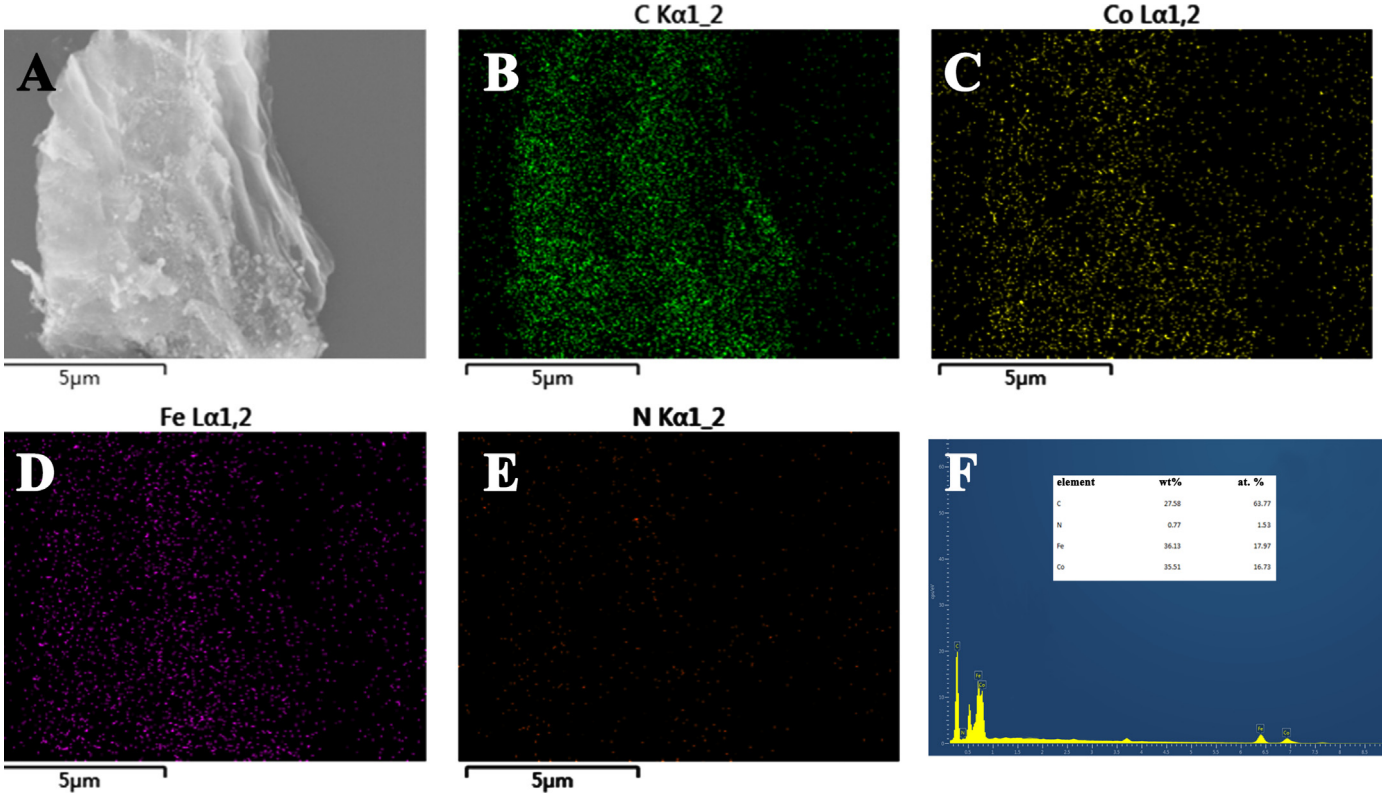

Fig. 3. Element mappings of (B) C, (C) Co, (D) Fe, and (E) N elements corresponding to the (A) SEM image of CoFe/NGR-2. (F) EDS spectrum of CoFe/NGR-2.

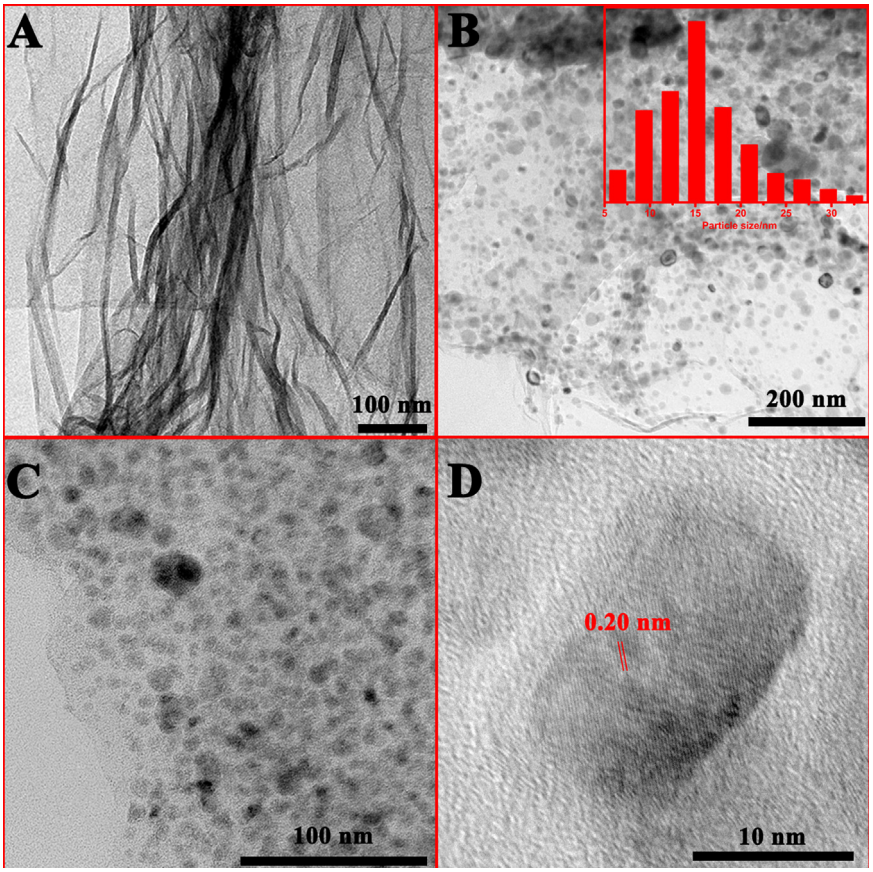

Fig. 4. TEM images of (A) NGR, (B and C) CoFe/NGR-2, and (D) HRTEM image of CoFe/NGR-2.

response of − 95.0, − 137.3 and − 115.6 μA, respectively. The peak potential for reduction of H_2O_2 at three CoFe/NGR electrodes is more positive than that at other electrodes. The higher reductive current and more positive peak potential observed from CVs suggest that three CoFe/NGR electrodes exhibit much better electrochemical activity towards H_2O_2. The anodic current is assigned to the electrochemical oxidation of H_2O_2 [1]. Generally, alloyed transition metals have been shown to tune the electronic properties at surface, Fermi level energy and subsequent adsorption behavior of intermediate, thus significantly enhancing electrocatalytic activity [53,54]. In this work, the Co and Fe metals possess different activities for H_2O_2 reduction. The combination of Co and Fe into composite electrocatalysts integrates the catalytic activities of both elements, thereby synergistically improving the electrocatalytic activity. The comparison between the CoFe-2 and CoFe/NGR-2 reflects that the NGR support can enhance the electrocatalytic ability through facilitating the support of CoFe-2 nanoparticles and accelerating the electron transfer. The powerful synergetic interaction between Co and Fe elements and the high conductivity of NGR integrates the catalytic properties of CoFe and structural properties of NGR, thus leading to the superior electrocatalytic performance towards the reduction of H_2O_2. The improvement effect of NGR in CoFe/NGR-2 is further supported by EIS method (Fig. S3). Compared with the CoFe-2, a small electric resistance is observed on CoFe/NGR-2 since the high conductivity facilitates the electron transfer. The combination of NGR and CoFe-2 nanoparticles into composites of CoFe/NGR-2 inherits unique properties of both materials and promotes the catalytic performance. As summarized in Fig. S4, the CoFe/NGR-2 shows higher catalytic current than other samples with the current response being 1.59, 4.03 and 10.31 times larger than Co/NGR, Fe_2N/NGR, and CoFe LDHs/GO-2. Additionally, CoFe/NGR-2 possesses a larger signal response than that of CoFe/NGR-1 and CoFe/NGR-3 perhaps due to the optimized Co/Fe ratio. In Fig. 7A and B, the current response at CoFe/NGR-2 increases linearly with the increase of concentration of H_2O_2 from 1 to 5 mM. The cathodic current increases with the increase of H_2O_2 concentration according to the following reaction equation:

$$H_2O_2 + 2H^+ + 2e^- \rightleftharpoons 2H_2O$$

Consistent with voltammetric data, a similar trend is found for the chronoamperometric current in which the CoFe/NGR-2 presents the higher reduction signal than other electrodes (Fig. 8A). The signal amplification indicates the better electrocatalytic activity of CoFe/NGR-2 compared to other electrodes. The current response is proportional to the concentration of H_2O_2 in the range of 100–400 μM (Fig. 8B-C). Fig. S5 shows the current responses of CoFe/NGR-2 in 0.1 M PBS with the pH varying from 5 to 9 in the presence of 5 mM H_2O_2. The peak currents towards the H_2O_2 reduction increase gradually and then almost reach a plateau at pH values of 7.4, 8 and 9. Therefore, the pH value of 7.4 was chosen as supporting electrolyte. After electrochemical recycling of CoFe/NGR-2 with cyclic voltammetry from 0.4 to − 0.8 for 100 cycles in the presence of H_2O_2, as evidenced by HRTEM image, the lattice of 0.20 nm corresponding to (110) plane of CoFe alloy is observed in both edge and core of CoFe nanoparticle (Fig. S6), suggesting the original composition of CoFe alloy is well retained. This result can be attributed to the potential range covering the oxidation and reduction of metallic alloy and moderate environments.

To optimize the effect of applied potential on electrochemical activity of CoFe/NGR-2, the electrochemical reduction of 10 μM H_2O_2 at CoFe/NGR-2 with different applied potential is compared in Fig. S7. Experimental results indicate that at the applied potential of − 0.25 V CoFe/NGR-2 exhibits much higher current than other potentials. Based on the optimized potential, Fig. 9A shows the current-time curve of CoFe/NGR-2 with successive additions of H_2O_2 at the potential of − 0.25 V. The CoFe/NGR-2 exhibits linear current responses to H_2O_2

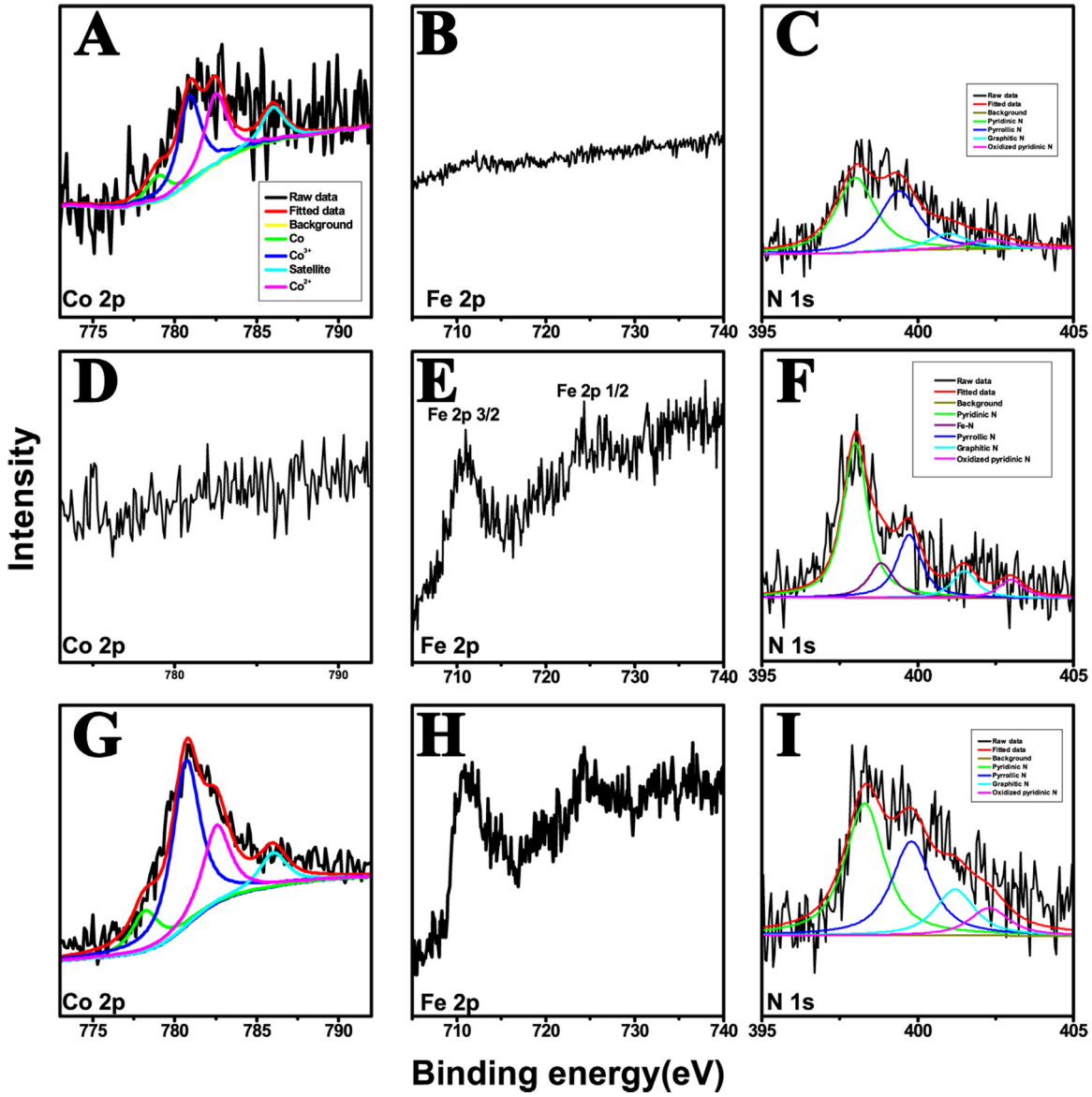

Fig. 5. XPS spectra of (A-C) Co/NGR, (D-F) Fe_2N/NGR, and (G-I) CoFe/NGR-2. (A, D and G) Co 2p spectra. (B, E and H) Fe 2p spectra. (C, F and I) N 1s spectra.

concentrations between 1 and 8654 μM (Fig. 9B, R = 0.9997, n = 36) with a sensitivity of 435.7 μA mM^{-1} cm^{-2} (normalized by geometric area of GC electrode). The detection limit is calculated to be 0.28 μM. In Table 1, a comparison of linear range, detection limit, response time, and sensitivity for CoFe/NGR-2 with other H_2O_2 sensors reported in literatures was summarized. The comparative results reflect the analytical performance of CoFe/NGR-2 are comparable to and even better than those recently electrodes. Another attractive feature of CoFe/NGR-2 is that the CoFe/NGR-2 responds very rapidly to the addition of H_2O_2, achieving steady-state signals within 1 s (Fig. 9C). Therefore, the CoFe/NGR-2 is a good candidate for preparation of amperometric sensor for H_2O_2 with prompt response, high sensitivity, and wide linear range.

In addition to the sensitivity, reproducibility and response time, stability and selectivity are also important parameters for evaluating the electrochemical sensors. First, the reproducibility of the sensor is measured by estimating the relative standard deviation (RSD) of current signal for 100 μM H_2O_2 for five electrodes. The RSD of five electrodes towards 100 μM H_2O_2 is calculated to be 7.9%. Additionally, the RSD of three sensitivities at the same electrode is found to be 4.8%. In Fig. 9D, the i-t curve shows the selectivity of the CoFe/NGR-2 towards 100 μM ascorbic acid (AA), 100 μM acetaminophen (AP), 100 μM dopamine (DA), and 100 μM uric acid (UA). Apparently, no current responses are found with the addition of AA, AP, DA, and UA. Conversely, CoFe/NGR-2 exhibits obvious current response upon the addition of H_2O_2. At this applied potential of − 0.25 V, the interferences can not be electrochemically reduced or oxidized at electrode surface, consequently avoiding the interference from these coexisting active species. In addition, when the CoFe/NGR-2 electrode is stored at 4 °C for three weeks, the current response towards 100 μM H_2O_2 remained 94.2% of its original value, suggesting the long-term stability of the electrode. The sensitivity remained 96.3% of its initial sensitivity, suggesting the long-term stability of the electrode.

The feasibility of CoFe/NGR-2 for H_2O_2 determination in real samples was evaluated by using standard addition method. The serum sample was diluted 2 times with 0.1 M PBS. The recoveries of H_2O_2 with concentrations of 100 and 200 μM were estimated to be 96.2% and 98.4%, respectively (Table 2). As indicated in Table 2, the analytical results obtained at CoFe/NGR-2 is in agreement with those determined by titration, reflecting that CoFe/NGR-2 can be used for determining H_2O_2 in real samples. The above results show that this new electrode is suitable for the detection of H_2O_2 in real sample. The feasibility of CoFe/NGR-2 in detection of H_2O_2 in real sample was evaluated by

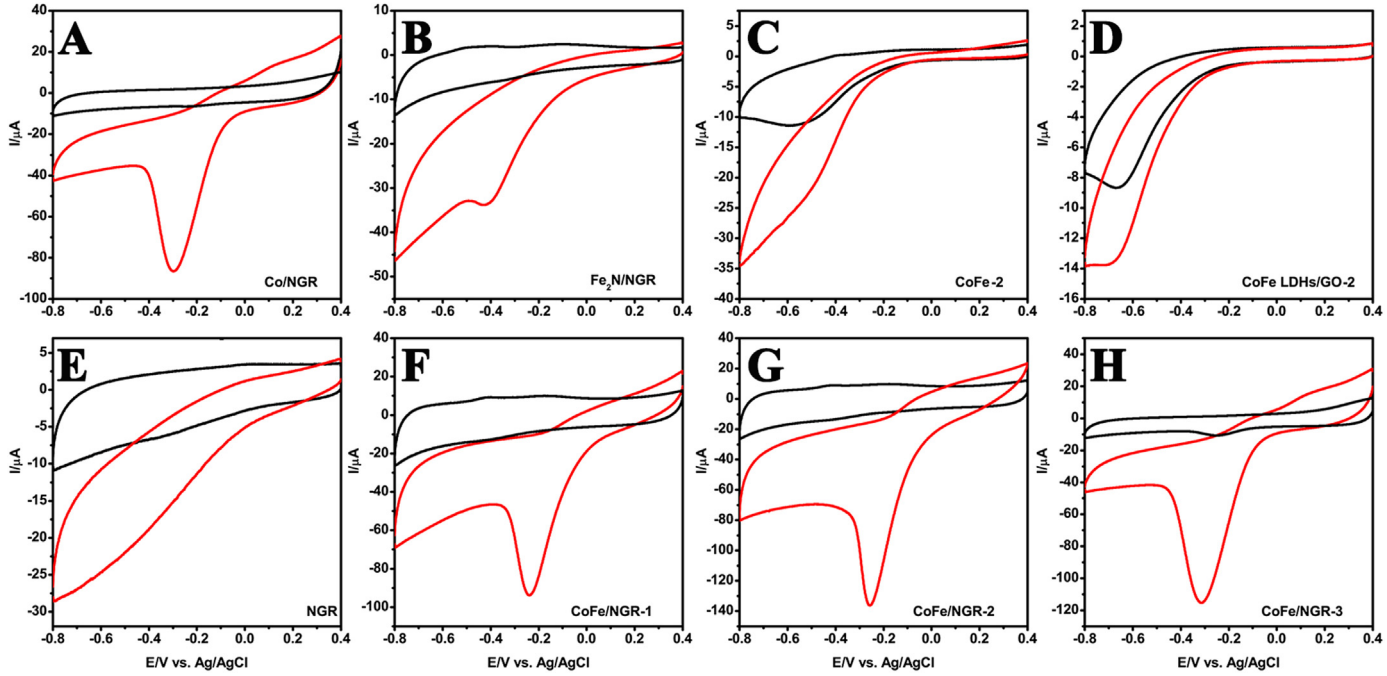

Fig. 6. CVs of (A) Co/NGR, (B) Fe_2N/NGR, (C) CoFe-2, (D) CoFe LDHs/GO-2, (E) NGR, (F) CoFe/NGR-1, (G) CoFe/NGR-2, and (H) CoFe/NGR-3 in 0.1 M PBS with (red) or without (black) 5 mM H_2O_2. Scan rate: 50 mV s^{-1}.

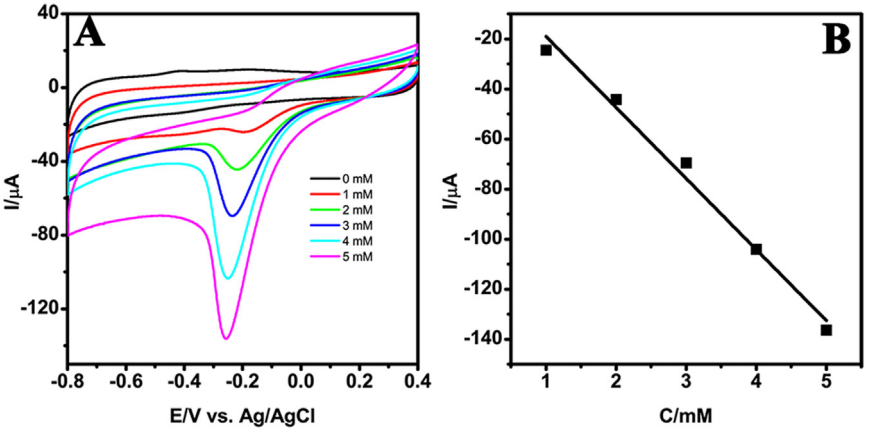

Fig. 7. (A) CVs of CoFe/NGR-2 in 0.1 M PBS with 1, 2, 3, 4, and 5 mM H_2O_2. (B) Calibration curve of CoFe/NGR-2 in the range of 1–5 mM H_2O_2.

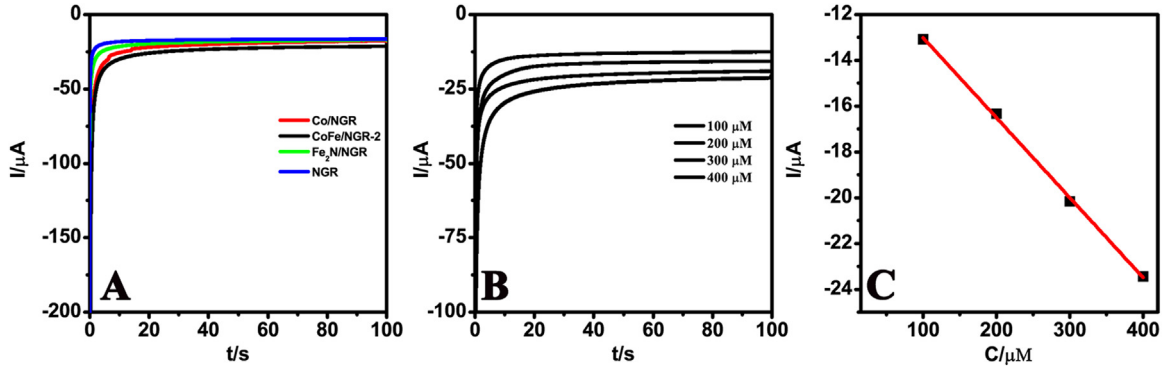

Fig. 8. (A) Chronoamperograms of Co/NGR, Fe_2N/NGR, CoFe-2, CoFe LDHs/GO-2, NGR, CoFe/NGR-1, CoFe/NGR-2, and CoFe/NGR-3 in 0.1 M PBS with 400 μM H_2O_2. (B) Chronoamperograms of CoFe/NGR-2 in the different concentration of H_2O_2. (C) Calibration curve of CoFe/NGR-2 in the range of 100–400 μM H_2O_2.

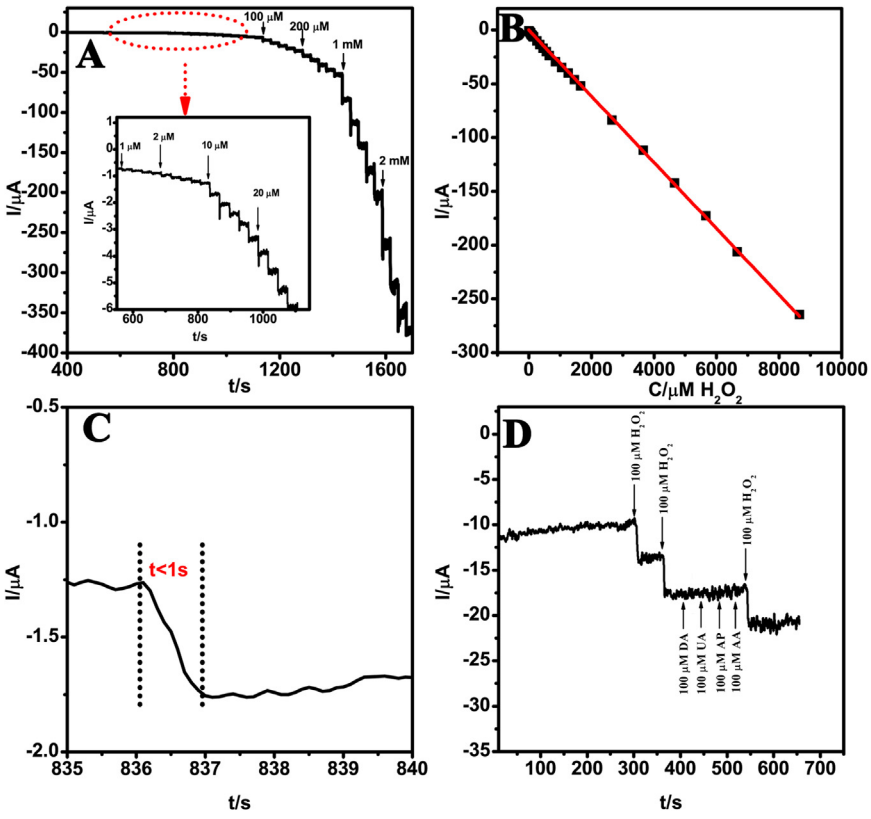

Fig. 9. (A) Current-time curve of CoFe/NGR-2 with successive additions of H_2O_2 at − 0.25 V. Inset shows the amplification of current-time curve with low concentration of 1, 2, 10, and 20 μM H_2O_2. (B) The corresponding calibration plot for CoFe/NGR-2. (C) The response time of CoFe/NGR-2 towards the H_2O_2. (D) The selectivity of CoFe/NGR-2 towards 100 μM AA, 100 μM UA, 100 μM AP, and 100 μM DA at the potential of − 0.25 V.

Table 1
The comparison of analytical performance of CoFe/NGR-2 with recently reported H_2O_2 sensor.

Electrode	Linear range (μM)	LOD (μM)	Response time (s)	Sensitivity (μA mM^{-1} cm^{-2})	Reference
N-Co-CNT@graphene	2.0–7449	2.0	–	28.66	[21]
FeOOH/carbon fiber paper	50–500	18	5	194	[31]
$SmCoO_3$	0.1–10,000	0.004	–	715	[11]
Co_3N/Ti mesh	2–28000	1	5	139.9	[43]
Cu_3N/copper foam	0.1–10000	0.009	3	7600	[44]
nickel borate/carbon cloth	0.1–500	0.85	3	18320	[33]
MnOOH/carbon cloth	20–9670	3.2	–	692.42	[29]
Co_3O_4/mesoporous carbon nanofibers	1–2580	0.5	4	72.75	[50]
ZnO/Co_3O_4/$NiCo_2O_4$	0. 2–2400	0.16	5	388	[64]
Co_3O_4/graphene oxide	0.05–400 450–1250	0.015	–	3450 2120	[19]
Graphite/Co_3O_4	1–70	0.0217	5	65.32	[65]
Co_3O_4 nanoparticles	0. 4–2200	0.105	3	959.79	[66]
Co_3O_4 nanowires/graphene	1.5–675	2.4	–	1140	[67]
Fe_3O_4/graphene	0.8–334.4	0.078	2.8	274.15	[68]
Fe_3O_4/mesoporous carbon	50–33080	5.89	5	77.07	[69]
horseradish peroxidase/Co_3O_4/GO	1000–30000	–	20	18.7	[70]
horseradish peroxidase/polydopamine/CNTs	1–2850	0.1	–	771	[71]
horseradish peroxidase/Pt/TiO_2	5–8000	1.36	3	–	[7]
CoFe/NGR − 2	1–8654	0.28	1	435.7	This work

Table 2
Determination of H_2O_2 in serum sample solutions (n = 3).

	Found (μM)	Added (μM)	After added (μM)	Recovery (%)	Estimated value by titration method (μM)
Sample 1	10.1	100	106.3 ± 4.6	96.2	113.2 ± 4.6
Sample 2	12.6	200	209.4 ± 8.9	98.4	216.1 ± 8.7

monitoring the concentration of H_2O_2 released from the living cells. CdTe QDs were used to stimulate the generation of H_2O_2 [61]. Fig. S8 compares the current responses obtained at CoFe/NGR-2 in the (a) absence and (b) presence of HeLa cells. In the presence of HeLa cells, the cathodic current suddenly increases with the addition of CdTe QDs (30 μL, 0.5 mg mL^{-1}). Upon the addition of catalase solution, the current decreases gradually, confirming the increased current signal is stemmed from the release of H_2O_2 in living cells stimulated by CdTe QDs. In contrast, no response is obtained after the same addition of CdTe QDs without HeLa cells. According to calibration curves in Fig. 9B, the concentration is calculated to be 0.47 μM. These results illustrate that CoFe/NGR-2 could be effectively used for reliable detection of H_2O_2.

In summary, the good analytical performance of CoFe/NGR-2 was attributable to the following factors: (1) Due to the high electrical conductivity of NGR, the electron transfer ability was distinctly

promoted at the electrode interface, thus favoring the electrochemical reduction of H_2O_2 at CoFe/NGR-2; (2) With the synergistic effect induced by Fe and Co elements in CoFe-2 nanoparticles, electrocatalytic activity is affected by the introduction of other metal component in the bimetallic system, thus exhibiting a promotion in current response. The combination of two aforementioned factors leads to superior analytical performance of CoFe/NGR-2 for H_2O_2 detection.

4. Conclusion

CoFe/NGR-2 was prepared by NH_3 treatment of CoFe LDHs/GO-2 composites. Compared with pure CoFe-2, the CoFe/NGR-2 displays a high activity towards the electrochemical reduction of H_2O_2. The enhanced performance was accredited to the excellent conductivity of NGR and synergistic interaction between the Co and Fe elements, accelerating the electron transfer between the H_2O_2 and electrode surface. Combining the catalytic properties of CoFe-2 nanoparticles and electric conductivity of NGR, the composite of CoFe/NGR-2 shows high analytical performance towards the H_2O_2 with wide linearity, fast response, low detection limit, and high sensitivity. This result suggests the CoFe/NGR-2 is a promising candidate for developing as a nonenzymatic H_2O_2 sensor.

Acknowledgements

The authors gratefully acknowledge the financial support by the National Natural Science Foundation of China (No. 21405011 and 21605015), the Development Project of Science and Technology of Jilin Province (20170101176JC), the Fundamental Research Funds for the Central Universities (2412017BJ003), the Recruitment Program of Global Youth Experts, the Jilin Provincial Department of Education, and the start-up funds from Northeast Normal University. We are grateful for the service support from Analysis and Testing Center of Northeast Normal University.

Appendix A. Supporting information

Supplementary data associated with this article can be found in the online version at http://dx.doi.org/10.1016/j.talanta.2018.06.003.

References

[1] R. Zhang, W. Chen, Recent advances in graphene-based nanomaterials for fabricating electrochemical hydrogen peroxide sensors, Biosens. Bioelectron. 89 (2017) 249–268.
[2] Y. Sheng, H. Yang, Y. Wang, L. Han, Y. Zhao, A. Fan, Silver nanoclusters-catalyzed luminol chemiluminescence for hydrogen peroxide and uric acid detection, Talanta 166 (2017) 268–274.
[3] W. Meisheng, C. Zhiqin, X. Hengyu, Z. Aiping, Sensitive electrochemiluminescence resonance energy transfer (ECL-RET) between $Ru(bpy)_3^{2+}$ and Au nanorod for hydrogen peroxide detection, Sci. China Chem. 60 (2017) 410–414.
[4] A. Rhouati, M. Nasir, J.-L. Marty, A. Hayat, Photoinduced discharge of electrons stored in a TiO_2-MWCNT composite to an analyte: application to the fluorometric determination of hydrogen peroxide, glucose and aflatoxin B1, Microchim. Acta 185 (2017) 26.
[5] Y. Liu, X. Liu, Z. Guo, Z. Hu, Z. Xue, X. Lu, Horseradish peroxidase supported on porous graphene as a novel sensing platform for detection of hydrogen peroxide in living cells sensitively, Biosens. Bioelectron. 87 (2017) 101–107.
[6] J. Chao, M. Zou, C. Zhang, H. Sun, D. Pan, H. Pei, S. Su, L. Yuwen, C. Fan, L. Wang, A MoS_2-based system for efficient immobilization of hemoglobin and biosensing applications, Nanotechnology 26 (2015) 274005.
[7] X. Wu, H. Zhang, K. Huang, Y. Zeng, Z. Zhu, Rose petal and P123 dual-templated macro-mesoporous TiO_2 for a hydrogen peroxide biosensor, Bioelectrochemistry 120 (2018) 150–156.
[8] H. Xia, J. Li, L. Ma, Q. Liu, J. Wang, Electrospun porous $CuFe_2O_4$ nanotubes on nickel foam for nonenzymatic voltammetric determination of glucose and hydrogen peroxide, J. Alloy. Compd. 739 (2018) 764–770.
[9] H. Chen, X. Wang, G. Liu, A. Lin, Y. Wen, H. Yang, Electrochemical construction of porous gold nanostructures on DVD substrate and its application as nonenzymatic hydrogen peroxide sensor, Sci. China Chem. 58 (2015) 1585–1592.
[10] W. Liu, K. Hiekel, R. Hübner, H. Sun, A. Ferancova, M. Sillanpää, Pt and Au bimetallic and monometallic nanostructured amperometric sensors for direct detection of hydrogen peroxide: influences of bimetallic effect and silica support, Sens. Actuators B 255 (2018) 1325–1334.
[11] J. He, W. Zhou, J. Sunarso, X. Xu, Y. Zhong, Z. Shao, X. Chen, H. Zhu, 3D ordered macroporous $SmCoO_3$ perovskite for highly active and selective hydrogen peroxide detection, Electrochim. Acta 260 (2018) 372–383.
[12] N. Yusoff, P. Rameshkumar, M.S. Mehmood, A. Pandikumar, H.W. Lee, N.M. Huang, Ternary nanohybrid of reduced graphene oxide-nafion@silver nanoparticles for boosting the sensor performance in non-enzymatic amperometric detection of hydrogen peroxide, Biosens. Bioelectron. 87 (2017) 1020–1028.
[13] L. Ning, X. Guan, J. Ma, M. Wang, X. Fan, G. Zhang, F. Zhang, W. Peng, Y. Li, A highly sensitive nonenzymatic H_2O_2 sensor based on platinum, $ZnFe_2O_4$ functionalized reduced graphene oxide, J. Alloy. Compd. 738 (2018) 317–322.
[14] L. Tian, K. Xia, W. Hu, X. Zhong, Y. Chen, C. Yang, G. He, Y. Su, L. Li, A wide linear range and stable H_2O_2 electrochemical sensor based on Ag decorated hierarchical Sn_3O_4, Electrochim. Acta 231 (2017) 190–199.
[15] H. Tian, H. Fan, J. Ma, L. Ma, G. Dong, Noble metal-free modified electrode of exfoliated graphitic carbon nitride/ZnO nanosheets for highly efficient hydrogen peroxide sensing, Electrochim. Acta 247 (2017) 787–794.
[16] Y. Shu, J. Xu, J. Chen, Q. Xu, X. Xiao, D. Jin, H. Pang, X. Hu, Ultrasensitive electrochemical detection of H_2O_2 in living cells based on ultrathin MnO_2 nanosheets, Sens. Actuators B 252 (2017) 72–78.
[17] P. Salazar, V. Rico, A.R. González-Elipe, Non-enzymatic hydrogen peroxide detection at NiO nanoporous thin film- electrodes prepared by physical vapor deposition at oblique angles, Electrochim. Acta 235 (2017) 534–542.
[18] S. Rostami, S.N. Azizi, S. Ghasemi, Using of silver nanoparticles incorporated in nanoporous ZSM-5 hierarchical zeolite prepared from bagasse as a new sensor for electrocatalytic determination of H_2O_2 in biological samples, J. Electroanal. Chem. 799 (2017) 583–594.
[19] S. Kogularasu, M. Govindasamy, S.M. Chen, M. Akilarasan, V. Mani, 3D graphene oxide-cobalt oxide polyhedrons for highly sensitive non-enzymatic electrochemical determination of hydrogen peroxide, Sens. Actuators B 253 (2017) 773–783.
[20] Y. Yuan, Y. Zheng, J. Liu, H. Wang, S. Hou, Non-enzymatic amperometric hydrogen peroxide sensor using a glassy carbon electrode modified with gold nanoparticles deposited on CVD-grown graphene, Microchim. Acta 184 (2017) 4723–4729.
[21] J. Balamurugan, T.D. Thanh, G. Karthikeyan, N.H. Kim, J.H. Lee, A novel hierarchical 3D N-Co-CNT@NG nanocomposite electrode for non-enzymatic glucose and hydrogen peroxide sensing applications, Biosens. Bioelectron. 89 (2017) 970–977.
[22] T. Liu, M. Li, P. Dong, Y. Zhang, L. Guo, Design and facile synthesis of mesoporous cobalt nitride nanosheets modified by pyrolytic carbon for the nonenzymatic glucose detection, Sens. Actuators B 255 (2018) 1983–1994.
[23] X. Yang, Y. Ouyang, F. Wu, Y. Hu, Y. Ji, Z. Wu, Size controllable preparation of gold nanoparticles loading on graphene sheets@cerium oxide nanocomposites modified gold electrode for nonenzymatic hydrogen peroxide detection, Sens. Actuators B 238 (2017) 40–47.
[24] S. Yang, G. Li, D. Wang, Z. Qiao, L. Qu, Synthesis of nanoneedle-like copper oxide on N-doped reduced graphene oxide: a three-dimensional hybrid for nonenzymatic glucose sensor, Sens. Actuators, B 238 (2017) 588–595.
[25] Z.L. Wu, C.K. Li, J.G. Yu, X.Q. Chen, MnO2/reduced graphene oxide nanoribbons: facile hydrothermal preparation and their application in amperometric detection of hydrogen peroxide, Sens. Actuators B 239 (2017) 544–552.
[26] Y. Shu, B. Li, Q. Xu, P. Gu, X. Xiao, F. Liu, L. Yu, H. Pang, X. Hu, Cube-like $CoSn(OH)_6$ nanostructure for sensitive electrochemical detection of H_2O_2 in human serum sample, Sens. Actuators B 241 (2017) 528–533.
[27] W. Meng, S. Xu, L. Dai, Y. Li, J. Zhu, L. Wang, An enhanced sensitivity towards H_2O_2 reduction based on a novel Cu metal–organic framework and acetylene black modified electrode, Electrochim. Acta 230 (2017) 324–332.
[28] D.S. achari, C. Santhosh, R. Deivasegamani, R. Nivetha, A. Bhatnagar, S.K. Jeong, A.N. Grace, A non-enzymatic sensor for hydrogen peroxide based on the use of α-Fe_2O_3 nanoparticles deposited on the surface of NiO nanosheets, Microchim. Acta 184 (2017) 3223–3229.
[29] W. Xu, J. Liu, M. Wang, L. Chen, X. Wang, C. Hu, Direct growth of MnOOH nanorod arrays on a carbon cloth for high-performance non-enzymatic hydrogen peroxide sensing, Anal. Chim. Acta 913 (2016) 128–136.
[30] W. Wu, Y. Li, J. Jin, H. Wu, S. Wang, Q. Xia, A novel nonenzymatic electrochemical sensor based on 3D flower-like Ni_7S_6 for hydrogen peroxide and glucose, Sens. Actuators B 232 (2016) 633–641.
[31] S. Du, Z. Ren, J. Wu, W. Xi, H. Fu, Vertical α-FeOOH nanowires grown on the carbon fiber paper as a free-standing electrode for sensitive H_2O_2 detection, Nano Res. 9 (2016) 2260–2269.
[32] J. Huang, H. Li, Y. Zhu, Q. Cheng, X. Yang, C. Li, Sculpturing metal foams toward bifunctional 3D copper oxide nanowire arrays for pseudo-capacitance and enzyme-free hydrogen peroxide detection, J. Mater. Chem. A 3 (2015) 8734–8741.
[33] Z. Wang, F. Xie, Z. Liu, G. Du, A.M. Asiri, X. Sun, High-performance non-enzyme hydrogen peroxide detection in neutral solution: using a nickel borate nanoarray as a 3D electrochemical sensor, Chem. Eur. J. 23 (2017) 16179–16183.
[34] P. Gao, D. Liu, Facile synthesis of copper oxide nanostructures and their application in non-enzymatic hydrogen peroxide sensing, Sens. Actuators B 208 (2015) 346–354.
[35] C.Y. Lin, C.T. Chang, Iron oxide nanorods array in electrochemical detection of H_2O_2, Sens. Actuators B 220 (2015) 695–704.
[36] K. Vasuki, K.J. Babu, S. Sheet, G. Siva, A.R. Kim, D.J. Yoo, G.G. kumar, Amperometric hydrogen peroxide sensor based on the use of $CoFe_2O_4$ hollow nanostructures, Microchim. Acta 184 (2017) 2579–2586.
[37] S. Cui, S. Gu, Y. Ding, J. Zhang, Z. Zhang, Z. Hu, Hollow mesoporous $CuCo_2O_4$ microspheres derived from metal organic framework: a novel functional materials for simultaneous H_2O_2 biosensing and glucose biofuel cell, Talanta 178 (2018)

788–795.
[38] J. Bai, X. Jiang, A facile one-pot synthesis of copper sulfide-decorated reduced graphene oxide composites for enhanced detecting of H_2O_2 in biological environments, Anal. Chem. 85 (2013) 8095–8101.
[39] D. Chirizzi, M.R. Guascito, E. Filippo, C. Malitesta, A. Tepore, A novel nonenzymatic amperometric hydrogen peroxide sensor based on CuO@Cu_2O nanowires embedded into poly(vinyl alcohol), Talanta 147 (2016) 124–131.
[40] M. Liu, R. Liu, W. Chen, Graphene wrapped Cu_2O nanocubes: non-enzymatic electrochemical sensors for the detection of glucose and hydrogen peroxide with enhanced stability, Biosens. Bioelectron. 45 (2013) 206–212.
[41] C. Cheng, Y. Huang, N. Wang, T. Jiang, S. Hu, B. Zheng, H. Yuan, D. Xiao, Facile fabrication of Mn_2O_3 nanoparticle-assembled hierarchical hollow spheres and their sensing for hydrogen peroxide, ACS Appl. Mater. Interfaces 7 (2015) 9526–9533.
[42] D. Liu, T. Chen, W. Zhu, L. Cui, A.M. Asiri, Q. Lu, X. Sun, Cobalt phosphide nanowires: an efficient electrocatalyst for enzymeless hydrogen peroxide detection, Nanotechnology 27 (2016) 33LT01.
[43] F. Xie, X. Cao, F. Qu, A.M. Asiri, X. Sun, Cobalt nitride nanowire array as an efficient electrochemical sensor for glucose and H_2O_2 detection, Sens. Actuators B 255 (2018) 1254–1261.
[44] Z. Wang, X. Cao, D. Liu, S. Hao, R. Kong, G. Du, A.M. Asiri, X. Sun, Copper-nitride nanowires array: an efficient dual-functional catalyst electrode for sensitive and selective non-enzymatic glucose and hydrogen peroxide sensing, Chem. Eur. J. 23 (2017) 4986–4989.
[45] L. Venosta, M.V. Bracamonte, M.C. Rodríguez, S.E. Jacobo, P.G. Bercoff, Comparative studies of hybrid functional materials based on different carbon structures decorated with nano-magnetite. Suitable application as platforms for enzyme-free electrochemical sensing of hydrogen peroxide, Sens. Actuators B 248 (2017) 460–469.
[46] F. Chekin, F. Teodorescu, Y. Coffinier, G.-H. Pan, A. Barras, R. Boukherroub, S. Szunerits, MoS_2/reduced graphene oxide as active hybrid material for the electrochemical detection of folic acid in human serum, Biosens. Bioelectron. 85 (2016) 807–813.
[47] Nhi S. Nguyen, G. Das, Hyon H. Yoon, Nickel/cobalt oxide-decorated 3D graphene nanocomposite electrode for enhanced electrochemical detection of urea, Biosens. Bioelectron. 77 (2016) 372–377.
[48] J. Balamurugan, T.D. Thanh, N.H. Kim, J.H. Lee, Facile fabrication of FeN nanoparticles/nitrogen-doped graphene core-shell hybrid and its use as a platform for NADH detection in human blood serum, Biosens. Bioelectron. 83 (2016) 68–76.
[49] S. Kumar, J.G. Sharma, S. Maji, B.D. Malhotra, Nanostructured zirconia decorated reduced graphene oxide based efficient biosensing platform for non-invasive oral cancer detection, Biosens. Bioelectron. 78 (2016) 497–504.
[50] Y. Ni, Y. Liao, M. Zheng, S. Shao, In-situ growth of Co_3O_4 nanoparticles on mesoporous carbon nanofibers: a new nanocomposite for nonenzymatic amperometric sensing of H2O2, Microchim. Acta 184 (2017) 3689–3695.
[51] H. Wang, H. Yuan, S. Sae Hong, Y. Li, Y. Cui, Physical and chemical tuning of two-dimensional transition metal dichalcogenides, Chem. Soc. Rev. 44 (2015) 2664–2680.
[52] Y. Jiao, Y. Zheng, M. Jaroniec, S.Z. Qiao, Design of electrocatalysts for oxygen- and hydrogen-involving energy conversion reactions, Chem. Soc. Rev. 44 (2015) 2060–2086.
[53] J. Hu, C. Zhang, X. Meng, H. Lin, C. Hu, X. Long, S. Yang, Hydrogen evolution electrocatalysis with binary-nonmetal transition metal compounds, J. Mater. Chem. A 5 (2017) 5995–6012.
[54] K. Ghanbari, Z. Babaei, Fabrication and characterization of non-enzymatic glucose sensor based on ternary NiO/CuO/polyaniline nanocomposite, Anal. Biochem. 498 (2016) 37–46.
[55] P.V. Suneesh, V. Sara Vargis, T. Ramachandran, B.G. Nair, T.G. Satheesh Babu, Co–Cu alloy nanoparticles decorated TiO_2 nanotube arrays for highly sensitive and selective nonenzymatic sensing of glucose, Sens. Actuators B 215 (2015) 337–344.
[56] L. Wang, Y. Zheng, X. Lu, Z. Li, L. Sun, Y. Song, Dendritic copper-cobalt nanostructures/reduced graphene oxide-chitosan modified glassy carbon electrode for glucose sensing, Sens. Actuators B 195 (2014) 1–7.
[57] H.-B. Noh, K.-S. Lee, P. Chandra, M.-S. Won, Y.-B. Shim, Application of a Cu–Co alloy dendrite on glucose and hydrogen peroxide sensors, Electrochim. Acta 61 (2012) 36–43.
[58] B. Yuan, C. Xu, L. Liu, Q. Zhang, S. Ji, L. Pi, D. Zhang, Q. Huo, Cu_2O/NiO_x/graphene oxide modified glassy carbon electrode for the enhanced electrochemical oxidation of reduced glutathione and nonenzyme glucose sensor, Electrochim. Acta 104 (2013) 78–83.
[59] H. Li, C.-Y. Guo, C.-L. Xu, A highly sensitive non-enzymatic glucose sensor based on bimetallic Cu–Ag superstructures, Biosens. Bioelectron. 63 (2015) 339–346.
[60] R. Ding, J. Liu, J. Jiang, J. Zhu, X. Huang, Mixed Ni-Cu-oxide nanowire array on conductive substrate and its application as enzyme-free glucose sensor, Anal. Methods 4 (2012) 4003–4008.
[61] J. Liu, X. Bo, Z. Zhao, L. Guo, Highly exposed Pt nanoparticles supported on porous graphene for electrochemical detection of hydrogen peroxide in living cells, Biosens. Bioelectron. 74 (2015) 71–77.
[62] Y. Xu, H. Bai, G. Lu, C. Li, G. Shi, Flexible graphene films via the filtration of water-soluble noncovalent functionalized graphene sheets, J. Am. Chem. Soc. 130 (2008) 5856–5857.
[63] Y. Wang, Z. Wang, Y. Rui, M. Li, Horseradish peroxidase immobilization on carbon nanodots/CoFe layered double hydroxides: direct electrochemistry and hydrogen peroxide sensing, Biosens. Bioelectron. 64 (2015) 57–62.
[64] B. Xue, K. Li, S. Gu, L. Zhang, J. Lu, Ni foam-supported ZnO nanowires and Co_3O_4/$NiCo_2O_4$ double-shelled nanocages for efficient hydrogen peroxide detection, Sens. Actuators B 262 (2018) 828–836.
[65] R.K. Das, A.K. Golder, Co_3O_4 spinel nanoparticles decorated graphite electrode: bio-mediated synthesis and electrochemical H_2O_2 sensing, Electrochim. Acta 251 (2017) 415–426.
[66] M. Wang, X. Jiang, J. Liu, H. Guo, C. Liu, Highly sensitive H_2O_2 sensor based on Co_3O_4 hollow sphere prepared via a template-free method, Electrochim. Acta 182 (2015) 613–620.
[67] L. Kong, Z. Ren, N. Zheng, S. Du, J. Wu, J. Tang, H. Fu, Interconnected 1D Co_3O_4 nanowires on reduced graphene oxide for enzymeless H_2O_2 detection, Nano Res. 8 (2015) 469–480.
[68] Y. Zhao, D. Huo, J. Bao, M. Yang, M. Chen, J. Hou, H. Fa, C. Hou, Biosensor based on 3D graphene-supported Fe_3O_4 quantum dots as biomimetic enzyme for in situ detection of H_2O_2 released from living cells, Sens. Actuators, B 244 (2017) 1037–1044.
[69] Z. Qin, Y. Zhao, L. Lin, P. Zou, L. Zhang, H. Chen, Y. Wang, G. Wang, Y. Zhang, Core/shell microcapsules consisting of Fe_3O_4 microparticles coated with nitrogen-doped mesoporous carbon for voltammetric sensing of hydrogen peroxide, Microchim. Acta 184 (2017) 4513–4520.
[70] S.A.B. Asif, S.B. Khan, A.M. Asiri, Electrochemical sensor for H_2O_2 using a glassy carbon electrode modified with a nanocomposite consisting of graphene oxide, cobalt(III) oxide, horseradish peroxidase and nafion, Microchim. Acta 183 (2016) 3043–3052.
[71] M. Dai, T. Huang, L. Chao, Q. Xie, Y. Tan, C. Chen, W. Meng, Horseradish peroxidase-catalyzed polymerization of l-DOPA for mono-/bi-enzyme immobilization and amperometric biosensing of H_2O_2 and uric acid, Talanta 149 (2016) 117–123.